Techniques to measure quantum criticality in cold atoms

Kaden R. A. Hazzard*
JILA and Department of Physics, University of Colorado, Boulder, Colorado 80309-0440, USA

Erich J. Mueller†
Laboratory of Atomic and Solid State Physics, Cornell University, Ithaca, New York 14853, USA

(Received 17 May 2011; published 11 July 2011)

We describe how rescaling experimental data obtained from cold atom density profiles can reveal signatures of quantum criticality. We identify a number of important questions which can be answered by analyzing experimental data in this manner. We show that such experiments can distinguish different universality classes and that the signatures are robust against temperature, noise, and finite system size.

DOI: 10.1103/PhysRevA.84.013604 PACS number(s): 03.75.Hh, 64.70.Tg

I. INTRODUCTION

A. General introduction

Attempts to understand zero temperature phase transitions have forced physicists to consider a regime where the standard paradigms of condensed matter physics break down [1–4]. These quantum critical systems lack a simple description in terms of weakly interacting quasiparticles and instead sport a range of exotic emergent properties. Most dramatically, theory predicts that universal scaling relationships describe their finite temperature thermodynamics, and this scaling persists up to remarkably high temperatures. Unfortunately, these universal functions are hard to calculate: for example, there are no reliable general techniques to calculate the scaling functions for dynamics [4,5]. Viewing a cold-atom experiment as a quantum simulator [6], we show how to extract universal scaling functions from (nonuniversal) atomic density profiles. Such experiments can resolve the important open question of the Mott-Metal crossover's dynamic exponent in the Fermi-Hubbard model [7,8] and explore the poorly characterized crossover between $O(2)$ and dilute Bose gas physics captured by the finite density $O(2)$ rotor model [1,9]. Such results would directly impact theories of, for example, high-temperature superconducting cuprates [10,11], heavy fermion materials [12], and graphene [13].

Several theoretical [14–17] and experimental [18] papers have appeared which address the same questions using similar techniques. In Sec. VI we explain in detail how the concepts introduced in these various papers interrelate.

Although our ideas are general, much of our discussion will focus on cold bosonic atoms, such as ^{87}Rb, trapped in optical lattices. Current experiments on this system are capable of observing quantum critical phenomena. This system displays multiple quantum phase transitions, which reside in distinct and nontrivial universality classes [1]. We will also discuss a number of other experimental realizations with rich quantum critical physics. Our protocols can be applied to any quantum phase transition and may even be useful outside of cold atoms.

B. Bose-Hubbard Model

Ultracold bosons in optical lattices are described by the Bose-Hubbard model [6,19,20], defined by the Hamiltonian

$$H = -t \sum_{\langle i,j \rangle} b_i^\dagger b_j + \sum_i \left[\frac{U}{2} b_i^\dagger b_i^\dagger b_i b_i - \mu b_i^\dagger b_i \right], \quad (1)$$

where $\sum_{\langle i,j \rangle}$ indicates a sum over nearest neighbors i and j, and the operators b_i and $b_i^\dagger$ annihilate and create bosons on site i. They satisfy the canonical commutation relation $[b_i, b_j^\dagger] = \delta_{ij}$. The parameters t and U are controlled by the depth V_0 of the optical lattice defined by $V(r) = V_0[\cos(2\pi x/\ell) + \ldots]$. Energies are typically measured in terms of $E_R = \hbar^2\pi^2/(2m\ell^2)$.

Figure 1(a) illustrates this model's phase diagram calculated within a finite temperature Gutzwiller approximation (see Appendix A). At low temperatures, it features a superfluid phase when the tunneling matrix element t is large compared to the on-site interaction U and a Mott insulating phase in the opposite limit. The superfluid phase is characterized by dissipationless mass transport, analogous to the dissipationless charge transport in a superconductor. It supports arbitrarily low-energy excitations and has an order parameter ψ that vanishes at the phase transition. The Mott insulating phase [lobes shown in Fig. 1(a)] can be caricatured as having a fixed integer number of particles per site, n, set by the chemical potential μ. The Mott insulating state has a excitation gap Δ, which vanishes at the transition.

The Mott insulating phase is strictly defined only at zero temperature, but a phase transition between a superfluid and a normal fluid persists to finite temperature.

Figure 1(b) illustrates a slice through the finite temperature phase diagram. This figure shows that the normal fluid is divided into three qualitatively distinct regions separated by smooth crossovers illustrated by dashed lines. At large t/U, the superfluid (SF) can be heated through a classical phase transition to a normal fluid (NF) with properties similar to that of a weakly interacting Bose gas. At small t/U, the low-temperature properties of the normal fluid (MI) are determined by the zero temperature Mott insulator's gap. A quantum critical region intervenes between these two normal fluids. Slices at fixed t/U look identical to slices at fixed μ/U.

*kaden.hazzard@colorado.edu
†em256@cornell.edu

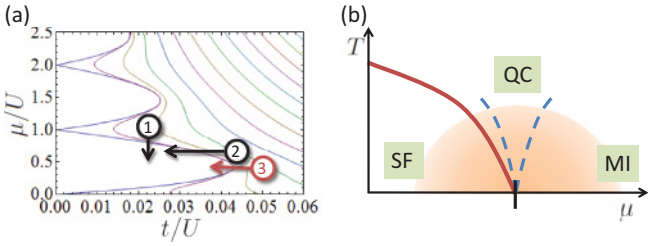

FIG. 1. (Color online) Quantum critical crossovers in the Bose-Hubbard model. (a) Normal (Mott insulator) to superfluid phase boundaries for (left to right) temperatures $T/U = 0.00, 0.06, 0.12, \ldots, 0.96$, calculated via finite temperature Gutzwiller mean field theory in $d = 2$. The parameters t, μ, and U are the tunneling rate, chemical potential, and on-site interaction energy of the Bose-Hubbard model, respectively. Paths (1,2) are governed by the dilute Bose gas universality class, and path (3) (passing through the tip) is governed by the $O(2)$ universality class. (b) Slice through the quantum phase transition at fixed t/U. Slices with fixed μ/U are similar. The abbreviations "SF," "MI," and "QC" denote the superfluid, Mott insulator-like normal fluid, and quantum critical regime, respectively, with the Mott insulator being strictly defined only at $T = 0$. The shaded region indicates where the physics is governed by the quantum critical point. The dashed lines represent smooth crossovers between the qualitatively distinct "QC" and "low temperature" regions. Deep in the former, T is the only relevant energy scale.

In fact, this structure is typical of all second-order quantum phase transitions: the disordered phase generically divides into an analogous set of three regions [1].

Sufficiently near the quantum phase transition [the shaded region in Fig. 1(b)], the thermodynamic functions obey scaling relationships. This scaling is typically controlled by two energy scales that vanish at the quantum critical point [1]. One scale is the temperature T, while the other depends on the phase: it is the zero temperature superfluid stiffness ρ_s in the superfluid and the gap to single particle excitations Δ in the Mott phase. Observables, such as the density, can be written as the sum of an nonuniversal part n_0 plus a function n_u that obeys the scaling form

$$n_u(T,\Delta) = T^{d/z}\Psi_n(\Delta/T). \tag{2}$$

Here, d is the dimension of the system and Ψ_n is a universal scaling function. Below an upper critical dimension d_c, the dynamical exponent z and the universal function Ψ_n are the same for a wide range of models and therefore define universality classes: here $d_c = 4 - z$, and z will be 1 or 2 depending on what part of the Mott lobe one is traversing. The nonuniversal contribution, $n_0(\mu,U,T)$, is the density of the system for $t = 0$, and as explained in appendix B is easily calculated or measured in independent experiments. Although atypical, with fine tuning it is possible to have situations where additional dimensionless parameters enter. The finite density $O(2)$ rotor model discussed below is one example.

II. PROPOSAL

A. Scaling from density profiles

Here, we introduce an experimental protocol to observe universality and measure key properties such as the dynamic critical exponent. Our technique relies upon the inhomogeneity of cold atoms experiments. Although typical observables in cold atoms, such as the density profile, are nonuniversal, we show that with appropriate analysis the absorption images of these trapped inhomogeneous clouds reveal the universal properties of corresponding homogeneous systems.

At first sight, this result is surprising. Given that critical points are associated with diverging length scales, one would naively expect that all features of criticality would be dominated by finite-size effects, and the properties of the trapped gas would be disjoint from those of the uniform gas. For example, Wessel *et al.* [21] found that in their Monte Carlo simulations of zero-temperature systems, critical properties *could not* be extracted from their density profiles. Similarly, studies of finite-temperature phase transitions typically find that it is difficult or impossible to extract any critical properties from density profiles [22–25]. These arguments, however, do not apply to the measurements we are advocating.

We propose searching for signatures of quantum criticality by comparing the density profiles of *finite temperature* clouds. As one increases the temperature, moving farther away from the quantum critical point, the correlation length drops. As we explicitly show in Sec. III, there is a sizable temperature range where the correlation length ξ is small compared to the cloud size L, yet one is still in a universal regime where all local thermodynamic properties are governed by the proximity to the quantum critical point. At these intermediate temperature scales, scaling relations such as Eq. (2) hold, *and* one can extract the equation of state from density profiles via a local density approximation.

In particular, if $\xi \ll L$, the cloud can be considered locally homogeneous, and at every point in space one may define a local pressure, density, and chemical potential. Standard hydrostatic equilibrium arguments [26,27] then force the chemical potential gradients to be balanced by trapping forces: $\mu(r) = \mu_0 - V(r)$. Hence, one can infer a great deal of information about the equation of state from a single-density image. The key problem we address is how quantum criticality is encoded in these density profiles.

We will view trapped atomic systems as locally satisfying Eq. (2), with a gap Δ that varies as a function of position in space. As already emphasized, our analytic and numerical results in trapped systems validate this Thomas-Fermi approximation. Direct measurement of $\Delta(\mathbf{r})$ is difficult in cold atoms. Instead, we will relate the gap to independently measurable thermodynamic quantities.

We illustrate our procedure by taking the compressibility $\kappa \equiv \partial n/\partial\mu$ as the independently measurable quantity. This is appealing because κ can be extracted directly from the density profiles via $\kappa = -(1/m\omega^2 r)\partial n/\partial r$ or from shot-to-shot fluctuations in the density [28,29]. Like the density, the compressibility is the sum of an easily determined nonuniversal part and a universal part, $\kappa = \kappa_0 + \kappa_u$, with

$$\kappa_u(T,\Delta) = T^{d/z-1}\Psi_\kappa(\Delta/T). \tag{3}$$

Equation (2) is an implicit equation for Δ, which together with Eq. (3) implies that

$$\kappa_u T^{1-d/z} = \Upsilon(n_u T^{-d/z}), \tag{4}$$

where $\Upsilon = \Psi_\kappa \circ \Psi_n^{-1}$ is a universal function. Therefore, in the quantum critical regime a graph of $\kappa_u T^{1-d/z}$ versus $n_u T^{-d/z}$ collapses onto a single curve independent of μ, t, U, T, and any other microscopic couplings.

B. Further Refinements

Several authors [14,15] have pointed out an important variant of this approach that can help pinpoint the critical point. Paralleling the technique often used in extracting critical points from numerical experiments on finite-sized systems, they suggest plotting $T^{-d/z} n_u$ as a function of μ. At the chemical potential of the quantum critical point all of these curves should cross.

III. NUMERICAL RESULTS

We validate our approach by applying it to data from "numerical experiments." We calculate density profiles of trapped atomic clouds and look for scaling properties. In Sec. III A we consider the 1D Bose-Hubbard model with where we are able to directly simulate the trapped system by mapping it onto noninteracting fermions. In Sec. III B we look at the 2D Bose-Hubbard model, using Monte Carlo techniques on small systems to infer the properties of the trapped gas.

A. 1D Bose-Hubbard Model

Figure 2(b) shows a plot of the scaled compressibility versus scaled density, extracted from the density profiles [Fig. 2(a)] of the $t/U \to 0$ (hard-core) trapped one-dimensional Bose-Hubbard model for $N = 70$ particles. These density profiles are efficiently calculated by mapping the system onto noninteracting fermions (see Appendix C). The figure not only demonstrates the universal collapse in the quantum critical regime but also validates the Thomas-Fermi approximation. The success of the Thomas-Fermi approximation is due to the fact that as one increases temperature above the quantum critical point the correlation length ξ shrinks, and throughout the quantum critical regime it is typically much smaller than the cloud size. As one approaches the classical phase transition, ξ diverges. Hence, even though our technique quite readily detects quantum criticality, signatures of the classical transition may be much harder to see [25].

As shown in Fig. 2(b), collapse occurs in a region around the quantum critical point but deviates at sufficiently large densities and temperatures. In this case, the data collapses within 10% for a density range of roughly $0.9 < n < 1.1$ and temperatures range of $T \lesssim t/4$. This is a generic feature of quantum criticality: the physics is universal only near the quantum critical point, with the size of the universal region determined by microscopic details.

The universal scaling functions in Fig. 2 correspond to those of the dilute Bose gas universality class (the same universality class that governs the edge of all cold bosonic clouds). Although this universality class is quantitatively understood [1,30], at larger t/U (near the tip of the lobe) the Bose-Hubbard

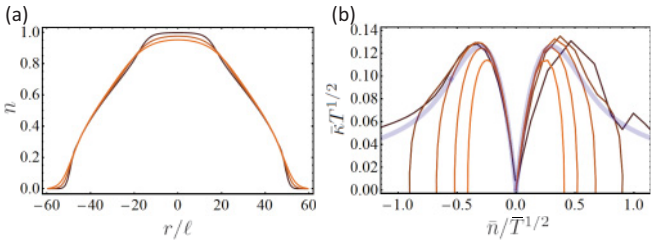

FIG. 2. (Color online) Extracting universal behavior and dynamical critical exponents from density profiles of the trapped one-dimensional Bose-Hubbard model. (a) Exact density profiles of the one-dimensional harmonically trapped hard-core Bose-Hubbard model for $N = 70$ particles at temperatures $\bar{T} \equiv T/t = 0.1, 0.24, 0.38$, with larger temperatures corresponding to lower central density. Here, r is the radial displacement in the trap and ℓ is the lattice spacing. These density profiles are nonuniversal; for example, they depend on temperature. (b) Our construction for obtaining universal scaling curves applied to this system, plotting $\bar{\kappa}\bar{T}^{d/z}$ versus $\bar{n}/\bar{T}^{1/z}$ (defining $\bar{\kappa} \equiv \kappa - \kappa_0$, $\bar{n} \equiv n - n_0$, and $\bar{T} = T/t$) for this $d = 1$, $z = 2$ transition and temperatures $\bar{T} = 0.1, 0.17, 0.24, 0.31, 0.38$ (from closest to the shaded grey band to farthest). The compressibility is approximated by $\kappa = \partial n/\partial\mu \approx (\partial n/\partial r)/(m\omega^2 r)$, where ω is the trap frequency, and $\partial n/\partial r$ is obtained by numerically differentiating the density. Lower temperatures display a larger region of collapse. We observe good collapse up to $T \sim 0.25t$, and see that the analysis accurately reproduces the homogeneous infinite system's scaling curve (shaded gray line) within $\lesssim 10\%$ for $T \lesssim 0.05t$ for the transition near $n = 1$ ($\bar{n} < 0$) and for $T \gtrsim 0.15t$ for the transition near $n = 0$ ($\bar{n} > 0$). This collapse occurs even for drastically different density profiles obtained by adjusting the trap depth in place of temperature (not shown). With moderately larger particle numbers ($N \sim 200$, not shown), the simulated data at low temperatures even more accurately reproduces the infinite homogeneous system's universal scaling function (the extracted curve lies within the shaded gray region).

model falls into the less trivial $O(2)$ universality class, for which open questions remain. In particular, the quantitative structure of the dynamic scaling functions is unknown and no general methods exist to compute these. Furthermore, there is a more intricate "finite density $O(2)$" universal structure governing the crossover between the $O(2)$ and dilute Bose gas universality classes, about which even less is known [9,13]. We give a simple picture of this physics and its relevance to the Bose-Hubbard model in Sec. IV B.

B. 2D Bose-Hubbard Model

Figure 3 shows that in addition to measuring universal scaling functions and the size of the universal region, our method enables one to distinguish the universality classes of the two-dimensional square lattice Bose-Hubbard model using only the density profiles. We calculate the equation of state $n(\mu)$ for a set of μ's realized in a typical cold atoms experiment, employing the numerically exact worm algorithm quantum Monte Carlo as implemented in the ALPS package [31]. To mimic the effect of the trapping potential, we calculated each density for a finite size 10×10 system. This length scale corresponds to a trapping potential variation of $\sim 1\%$ along the radial direction under typical conditions. We calculate $\kappa(\mu)$

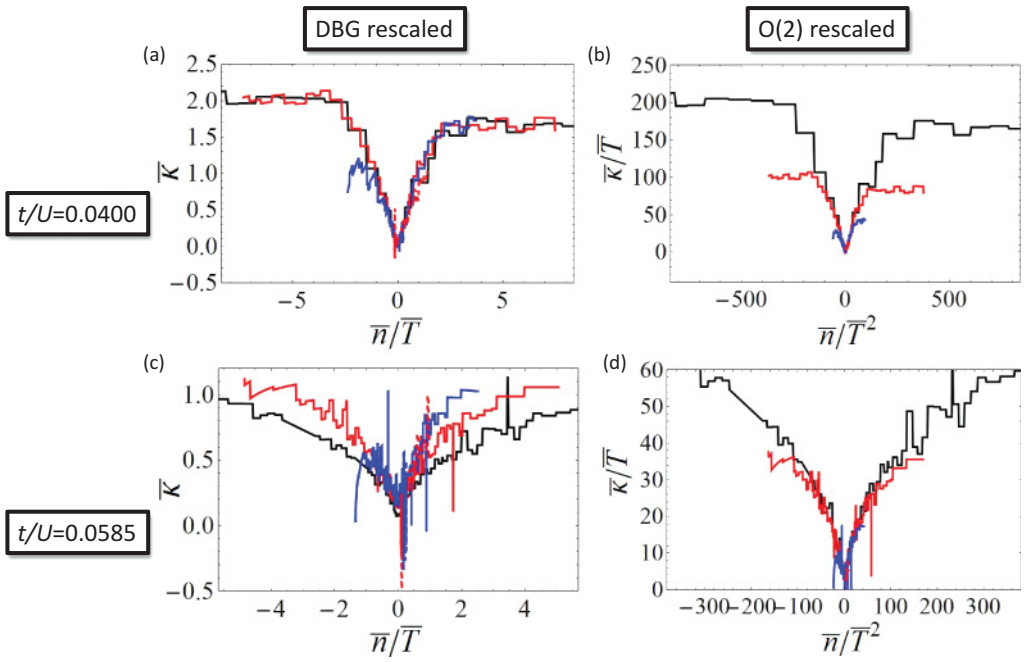

FIG. 3. (Color online) Extracting universal behavior and dynamical critical exponents from density profiles of the trapped two-dimensional Bose-Hubbard model. Each panel shows an application of our analysis procedure to simulated density profiles (as described in text) for temperature $T/t = 1/4, 1/2, 1, 2$, and 4 using the data in a density range $|n - 1| < 0.15$. The symbols $\bar{n}$, $\bar{\kappa}$, and $\bar{T}$ are defined in the legend of Fig. 2. Lower temperature curves are identified by noting that they span a wider $\bar{n}$ range. On the left (a and c), we plot $\bar{\kappa}$ versus $\bar{n}\bar{T}^{-1}$, while on the right (b and d) we plot $\bar{\kappa}\bar{T}^{-1}$ versus $\bar{n}\bar{T}^{-2}$: these will show collapse if the dynamical critical exponent is, respectively, $z = 2, 1$. Top (a and b) shows data with $t/U = 0.0400$, which should be described by the dilute Bose gas universality class ($z = 2$). Bottom (c and d) shows data with $t/U = 0.0585$, which should be better described by the $O(2)$ rotor model universality class ($z = 1$): the tip of the $n = 1$ Mott lobe in the homogeneous system is at $t/U = 0.0593$. As expected, we see collapse in (a) and (d). The scatter in data points corresponds to stochastic noise in our Monte Carlo simulations amplified by the differentiation. This noise is of comparable size to what would be seen in an experiment.

using the lowest-order finite difference derivative on this data. The stochastic error in the quantum Monte Carlo yields results with some noise ($\sim 0.1\%$), similar to that found applying finite differences to real experimental data ($\sim 1\%$ noise in radially averaged density profiles, e.g., in Gemelke *et al.*'s experiments [28]). Appendix E gives a discussion of signal-to-noise issues and more details about numerical parameters. Larger scale simulations of the trapped system [15] verify that this approach correctly captures the physics of criticality in the trapped gas.

The values $t/U = 0.01, 0.0585$ shown in Fig. 3 correspond to lattice depths of $V_0/E_R = 18.1, 11.4$, respectively, for ^{87}Rb in a lattice with spacing $\ell = 532$ nm. This is found by numerically solving the noninteracting lattice problem and using the relations [20] $t = -\int d^3r\, w(\mathbf{r} - \mathbf{r_i})[-\frac{\hbar^2}{2m}\nabla^2 + V(\mathbf{r})]w(\mathbf{r} - \mathbf{r_j})$ and $U = \frac{4\pi\hbar^2}{m} a \int d^3r\, |w(\mathbf{r})|^4$, where $w(\mathbf{r})$ is the Wannier state, and $\mathbf{r_i}, \mathbf{r_j}$ are the locations of neighboring sites.

Figure 3 shows that for $t/U = 0.0400$ the compressibility vs. density curves collapse if we use a dynamical critical exponent $z = 2$, corresponding to the dilute Bose gas universality class. Similarly, the $t/U = 0.0585$ data collapses if we use $z = 1$, as one expects for the $O(2)$ universality class. Like Fig. 2, the collapse occurs only sufficiently close to the critical point. The behavior persists up to temperatures on the order of $\gtrsim t$ and for a density range of roughly $0.9 < n < 1.1$. Since we are at the upper critical dimension of the dilute Bose gas model, we expect logarithmic corrections to scaling that are hard to identify on these plots. Consistent with our discussion of the Thomas-Fermi approximation's validity, there is no clear signature of the classical phase transition in these graphs.

IV. OUTLOOK

In this section we discuss how these techniques can be used to answer important questions about the quantum critical behavior of systems of interest to condensed matter physics. The most exciting direction is to apply our method to Fermi lattice systems [32,33], for example, those emulating the two-dimensional square lattice Fermi-Hubbard model. There are also some interesting open questions in the dynamical response functions of the finite-density $O(2)$ model.

A. Fermi-Hubbard Model

As a first example of important questions that can be addressed by these techniques, we propose studying the nature of the Mott-metal crossover in the Fermi-Hubbard model at temperatures $t^2/U \ll T \ll t$. Many believe that in real materials, such as transition metal oxides, this crossover is a manifestation of a preempted quantum critical regime and should display universal physics analogous to that of the Bose-Hubbard model's normal fluid to Mott insulator crossover (see the discussion in Refs. [1,7]). If one analyzes the square lattice fermion density profiles with the procedure we have introduced and sees collapse onto universal curves, it would

be compelling evidence that in the Fermi-Hubbard model the crossover is governed by a quantum critical point. Although most current experiments [32,33] are three-dimensional, and thus likely above the upper critical dimension, signatures of scaling (only with mean-field exponents) would remain if this quantum criticality is the correct description of the crossover. If the quantum critical regime persists to the same temperature scales as the Bose-Hubbard model, then current atomic experiments are already sufficiently cold to determine if the universal Mott-metal crossover scenario is correct.

Beyond determining if the system is critical, this analysis would also provide the dynamical critical exponent: a quantity whose value is currently unknown for many models, including the 2D square lattice Fermi-Hubbard model.

Depending on the character of the metallic state, some filling-controlled Mott-metal transitions display $z = 2$, while others display $z = 4$ [7]. To determine this exponent, one would analyze two-dimensional lattice fermions' density profiles with our scaling techniques: only when z is chosen correctly will collapse occur, and thus our protocol is capable of distinguishing between the various theoretical scenarios. As we already argued, the present generation of experiments is already in the correct regime to conduct such studies. Future experiments at lower temperatures $T \ll t^2/U$ will be able to access even more exotic features of quantum criticality.

One can explore an even broader range of open questions if in addition to measuring density profiles one also employs spectroscopic probes to measure dynamical response functions. For example, for lattice systems, experimentalists have successfully measured modulation spectra [34], Bragg spectra [35], and radio-frequency spectra [36]. In the quantum critical regime, these response functions satisfy universal scaling forms $\chi(\omega, T, \Delta) = T^{\eta}\Psi_{\chi}(\Delta/T, \omega/T)$. In both fermionic and bosonic systems, the details of these dynamic scaling functions are largely unknown, especially the low-frequency dynamic behavior and how it connects to higher frequency behavior. Note, however, that the Thomas-Fermi approximation's validity for spectra in the quantum critical regime has not been explicitly checked in our work, and its validity as well as other issues such as sufficient signal-to-noise remain open questions.

Up to this point, all of our discussion has focused on what can be achieved with present experimental capabilities. As experiments reach lower temperatures, our analysis technique can be used to probe ever more fundamental physics. For example, one can argue that even the simplest symmetry breaking transitions of a Fermi liquid, that to a spin density wave, is ill-understood: beyond the Hertz-Millis theory, there exist an infinite number of marginally relevant coupling constants and its universality class is unclear [37,38]. By measuring density profiles in a system displaying similar quantum phase transitions, such as dipolar fermions' transition to a Wigner crystal (charge density wave) or near-resonant fermions transition to an "FFLO" state (charge density wave + superfluid order), our techniques can measure z and thus provide valuable information about these transitions' universality classes. Additionally, the competing instabilities (e.g., to d-wave superconductivity, nematicity, etc.) seen in transition metal oxides have analogs in lattice fermion experiments and offer an important and even richer set of open questions regarding quantum critical behavior and "avoided quantum criticality" [2–5,39].

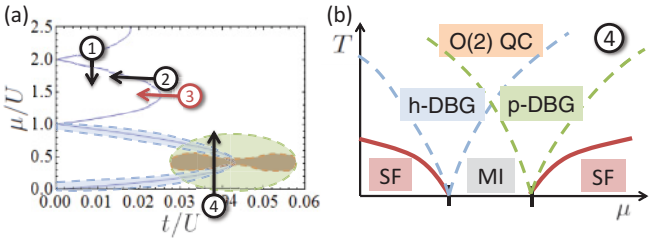

FIG. 4. (Color online) Universality classes of the Bose-Hubbard model. (a) Annotated zero temperature Bose-Hubbard model phase diagram (cf. Fig. 1). Transitions via paths (1-2) are described by the dilute Bose gas (DBG) universality class while path (3) is described by the $O(2)$ universality class. Shaded regions schematically depict where each universality class holds: DBG physics governs the (blue) region along the lobe edge and $O(2)$ rotor physics governs the (orange) "bowtie"-shaped region near the tip. The entire (green) region in the area around the tip—including both the bowtie and part of the lobe edge—is described by the finite density $O(2)$ model. (b) Finite temperature phase diagram along path (4). At zero temperature, this path crosses two quantum phase transitions going from a superfluid to a Mott insulator fs and back. Each phase transition is in the DBG universality class and displays a quantum critical fan, inside of which the temperature sets the only length scale. $O(2)$ physics is recovered in the particle-hole symmetric regions where the quantum critical fans overlap. The "finite density $O(2)$" model universally governs this entire phase diagram including all of the crossovers (dashed lines) and phase transitions (solid lines) shown in this panel.

B. Finite-density $O(2)$ model

A second area where one can advance our understanding of quantum criticality is through studying the "finite-density $O(2)$ model." This rich model describes the Bose-Hubbard model near the particle-hole symmetric point on the superfluid-insulator boundary. It features phase transitions in two different universality classes and a crossover between them. Sachdev and Müller have argued that aspects of the dynamics in this regime are related to dynamics near the Dirac point in graphene [13], and cold atoms may probe (among other things) the general relations between universal constants that should appear in both cases.

Figure 4 gives a guide to the relevant physics, illustrating the two universality classes and the crossovers between them. Along the Mott lobe edges, the physics is that of the dilute Bose gas [Fig. 4(a), shaded blue regions]. On the large-μ side of the Mott lobe, the relevant excitations are a dilute Bose gas of particles, while on the small-μ side, they are holes. Near the line of particle-hole symmetry passing through the tip of the lobe, both particles and holes are equally important and the physics is in the $O(2)$ universality class [Fig. 4(a), shaded orange region].

The physics of these regions, and the crossovers between them [the entire shaded green region in Fig. 4(a)] can be described by the imaginary time action $S = \int d^d r d\tau \mathcal{L}(\mathbf{r}, \tau)$

defined by the Lagrangian

$$\mathcal{L} = -\phi^*[(\partial_\tau - \mu)^2 - c^2\nabla^2 + s]\phi + \frac{g}{2}|\phi|^4, \qquad (5)$$

where ϕ is a complex bosonic field, evaluated at position $\mathbf{r}$ and time τ. Here, μ is the chemical potential, which controls the relative energy cost of holes and particles, s is the tuning parameter for the $\mu = 0$ phase transition, c the excitation velocity when $\mu = 0$, and g is the effective interaction strength. When μ is nonzero, at sufficiently low energies this reduces to the dilute Bose gas Lagrangian, $\mathcal{L}_{\mathrm{DBG}} = \psi^*[\partial_\tau - \mu - \nabla^2/(2m)]\psi + (g/2)|\psi|^4$ (with ψ a simple rescaling of ϕ), since the quadratic time derivative is *irrelevant* in the renormalization group sense. When $\mu = 0$, this reduces to the $O(2)$ model defined by the Lagrangian $\mathcal{L}_{O(2)} = \phi^*(-\partial_\tau^2 - c^2\nabla^2 + s)\phi + (g/2)|\phi|^4$. The model defined by Eq. (5) predicts a scaling function [9,40,41]

$$n_u(\Delta_+, \Delta_-, T) = T^d \Psi_{O(2)+\mu}\left(\frac{\Delta_+}{T}, \frac{\Delta_-}{T}\right), \qquad (6)$$

where $\Delta_\pm$ are the relevant gaps/superfluid stiffnesses at $T = 0$. This scaling function is universal and reduces to the dilute Bose gas and $O(2)$ scaling in the appropriate limits.

To see this reduction in the dilute Bose gas case, note that if for large Δ_-/T the scaling function goes to $\Psi(\Delta_+/T, \Delta_-/T) \to (\Delta_-/T)^{d/2}\Psi_r(\Delta_+/T)$, then $n_u \to T^{d/2}\Delta_-^{d/2}\Psi_r(\Delta_+/T)$. This reproduce the $z = 2$ scaling expected for the resulting dilute Bose gas case if $\Psi_n(\Delta_+/T) = \Delta_-^{d/2}\Psi_r(\Delta_+/T)$ is identified as the universal dilute Bose gas scaling function introduced in the main text.

A particularly insightful way to view the finite density $O(2)$ crossovers is illustrated in Fig. 4(b). This corresponds to a slice through Fig. 4(a) in the region described by Eq. (6). The low-temperature behavior is dominated by the two dilute Bose gas quantum critical points, and the $O(2)$ physics emerges at higher temperatures where the two fans overlap. Not only does the scaling in Eq. (6) describe the physics in these fans, it also describes the low-temperature phases.

V. FURTHER CONSIDERATIONS

Here, we discuss a few somewhat tangential points: other probes of quantum criticality, other examples of cold atom systems with quantum critical points, and finite-size scaling.

A. Time of flight expansion

As suggested by the work of Kato *et al.* [42], time of flight expansion provides another probe of quantum criticality. In such an experiment the trapping potential and interactions are turned off and the cloud is allowed to expand. At long times this maps the momentum distribution of the particles to the real-space distribution. At low momenta, the system's behavior is fully universal. Kato *et al.* [42] show a representative calculated image of the momentum distribution in a quantum critical regime of the Bose-Hubbard model.

In typical cold-atom experiments, the inhomogeneous broadening from the trap makes it very difficult to extract quantum critical signatures from the expansion images: multiple regions of the trap contribute to the observed momentum distribution, including those far from the quantum critical regime (although the critical coupling value may be extracted; see, e.g., Trotzky *et al.* [24] and Pollet *et al.* [25]). This difficulty can be somewhat circumvented by engineering a flat-bottomed trapping potential. Such flat traps may also be advantageous for density probes of quantum criticality.

B. Other cold atoms systems displaying quantum criticality

Here, we provide a partial list of other quantum phase transitions in cold-atoms systems. The most experimentally mature systems are: magnetic transitions in spinor gases [43], nematic transitions in dipolar gases [44], superfluid and magnetic transitions in partially polarized resonant Fermi gases [45], and transitions from fully polarized or fully paired phases to a partially polarized (FFLO) phase in one-dimensional clouds of fermions [46]. There are also potentially a large variety of transitions between magnetic phases in multicomponent gases and mixtures [6]. Finally, there are ample opportunities to study the *trivial* dilute gas to vacuum transitions, governed by the chemical potential tuned zero-temperature phase transition from a state with nonzero to zero density. This physics is found near the edge of every atomic cloud. Although well understood, these latter transitions are a good test of the analysis techniques.

Universal scaling behavior has already been experimentally studied in the two-dimensional dilute trapped Bose gas using techniques related to the ones we discuss here [47]. In the two-dimensional Bose system that they were looking at, dimensional analysis alone suffices to provide the collapse: all of the irrelevant couplings are zero in the bare Hamiltonian describing this system.

C. Finite-size scaling

We found by exact calculations of the trapped 1D hard-core Bose-Hubbard model (and by mimicking the trapped 2D Bose-Hubbard model) that our procedure could extract the homogeneous system's universal scaling function within a $\lesssim 10\%$ accuracy assuming the Thomas-Fermi approximation holds, despite the finite particle number and trapping inhomogeneity. Nevertheless, it is possible to improve this further by accounting for the finite-size scaling in the trap [14,25,48]. The trapping potential introduces a length scale L, and when this length is large compared to microscopic lengths, universal scaling in ξ/L^θ for some nontrivial θ results. For small values of this argument, the homogeneous system scaling is recovered. Accounting for this, some have explicitly demonstrated how to improve the accuracy of the naive Thomas-Fermi approach to determining critical coupling values (e.g., μ_c and T_c) [14,25].

VI. OTHER RECENT WORK

Given the excitement surrounding the possibility of observing quantum criticality in cold atoms, the field has evolved substantially since this manuscript was first circulated as a preprint. Most importantly, scaling collapse has been observed in density profiles from a recent set of experiments on cesium atoms trapped in optical lattices [18]. Further, sophisticated

numerical simulations have confirmed the results we showed in Sec. III B. A fair amount of progress has also been made in understanding signatures of quantum criticality in the 1D gas. Guan and Ho [16] have used approximate solutions of the thermodynamic Bethe ansatz to study attractive fermions.

We would like to give special attention to Zhou and Ho's recent Letter, which gives very similar arguments to those given here [14]. Given the similarities, we feel compelled to enumerate the differences between our works. This comparison also provides an opportunity to summarize our results. We owe several refinements of our arguments to discussions with Zhou and Ho, and we believe it is quite likely that their work was influenced to some extent by our results.

The main purpose of both our paper and Zhou and Ho's is to present techniques for observing universal collapse near a quantum critical point. We advocate plotting density vs. compressibility, while Zhou and Ho recommend density vs. chemical potential. While both are viable approaches, we feel that the primary benefit of our method is that both n and κ are local observables. In contrast, μ can only be determined if one knows the central chemical potential μ_0. In principle, μ_0 can be extracted by fitting the density profile at the edge of the cloud where the equation of state is simple. In practice, there are technical issues with this approach, including the fact that one must have the *entire cloud* in global equilibrium. In our method, one only needs equilibrium in the part of the cloud contributing to the critical region [49,50]. As a technical aside, Zhou and Ho's scaling prefactors (powers of temperature) look more complicated than ours; however, as discussed in Appendix D, since density is a conserved quantity their results reduce to ours. For other observables, one must use their more general form.

In order to show that our techniques are practical, both our paper and Zhou and Ho's use numerical simulations to model a trapped gas. These studies show that finite-size effects are small in current experiments, and signal-to-noise levels are sufficiently high. While both papers include discussion of the $d = 1$ Bose-Hubbard model in the hard-core limit, ours also looks at $d = 2$ and $U < \infty$. This lets us demonstrate that our technique can distinguish different universality classes and explore the interplay between $O(2)$ and dilute Bose gas physics.

Finally, our paper gives a number of concrete and nontrivial open questions involving quantum criticality, which can be studied in the near term by cold-gas experiments. These include determining the dynamical critical exponent for the Mott-metal crossover, the dynamics of the finite-density $O(2)$ model, and the validity of Hertz-Millis theory to describe various symmetry breakings of strongly interacting Fermi liquids.

Zhou and Ho's paper also contains important results that are not found in our paper—namely a study of finite-size scaling, a procedure to find the critical chemical potential of quantum phase transitions, and some discussion of classical phase transitions. We found that reading their paper also helped us view technical aspects of our procedure in a novel light and helped us improve our approach to subtract off the nonuniversal contribution to the density.

VII. CONCLUSIONS

We have shown that universal quantum critical behavior can survive in trapped cold atomic systems for realistic experimental conditions. We showed that from appropriate analysis of nonuniversal *in situ* density images, one can infer universal quantum critical scaling functions. To demonstrate this, we exactly calculated the expected behavior of the trapped Bose-Hubbard model in the hard-core 1D limit and in general in 2D, mimicking the trap with small finite-system sizes. We also demonstrated on the 2D Bose-Hubbard model that the procedure allows one to identify the dynamic critical exponent z and thus distinguish many important universality classes.

Using these results, we outlined how the techniques can be used with ongoing experiments on fermionic and bosonic atoms in optical lattices. We have shown that fermionic lattice experiments can answer important open questions regarding the Fermi-Hubbard model's universality class at intermediate temperatures. We have also argued that the bosonic lattice experiments can determine for the first time the quantitative structure of the dynamics of the finite-density $O(2)$ rotor model. We have also mentioned other open questions that ongoing cold atoms experiments can impact. Lastly, we outlined some of the very recent theoretical and experimental progress in the field.

ACKNOWLEDGMENTS

We thank Mukund Vengalattore, Stefan Baur, Stefan Natu, Sourish Basu, Srivatsan Chakram, Eun-Ah Kim, Cheng Chin, Nate Gemelke, Ben Machta, Qi Zhou, Jason Ho, Ed Taylor, Victor Gurarie, Nikolay Prokofiev, Lode Pollet, and Subir Sachdev for discussions. This work was supported by the National Science Foundation through Grant PHY-0758104 and by a grant from the Army Research Office with funding from the DARPA OLE program.

APPENDIX A: FINITE TEMPERATURE GUTZWILLER THEORY

We calculated the schematic finite temperature phase diagram in Fig. 1 within a finite temperature Gutzwiller approximation. Although only approximate, this approach provides a qualitative picture of the role of temperature. More accurate phase diagrams can be obtained by using quantum Monte Carlo techniques.

Following Fisher *et al*. [19] and Sachdev [1], we perform a Hubbard-Stratonovitch transform to decouple lattice sites: we introduce a novel free field ϕ into the Bose-Hubbard Lagrangian and couple it to the b operators by terms $-\sum_i (b_i^\dagger \phi_i^\dagger + \text{H.c.})$. The novel fields' Lagrangian is chosen so that upon integrating out ϕ, the original Bose-Hubbard Hamiltonian is reproduced. This field ϕ can be interpreted as the order parameter of the superfluid state. We formally integrate out the b fields and expand the Lagrangian for the ϕ fields to quartic order in ϕ and second order in derivatives to obtain

$$\mathcal{L}_\phi = \mathcal{L}_0 + \phi^* \left(s + K_1 \partial_\tau + K_2 \partial_\tau^2 - \nabla^2\right)\phi + u/2|\phi|^4, \quad \text{(A1)}$$

where the constants s, $\mathcal{L}_0$, K_1, K_2, and u can be expressed as integrals ($\mathcal{L}_0$ will give a nonuniversal contribution to the free energy considered in the next part). The mean field phase boundary is given by setting $s(T) = 0$. At $T = 0$, this reproduces the standard Gutzwiller theory. The explicit form for s is

$$s(T) = \frac{1}{zt} + \frac{1}{\mathcal{N}}\left[\sum_{m=0}^{\infty} \frac{m+1}{Um-\mu}(e^{-\beta(U/2)m(m-1)+\beta\mu m} - e^{-\beta(U/2)m(m+1)+\beta\mu(m+1)})\right], \tag{A2}$$

with $\mathcal{N} \equiv \sum_{m=0}^{\infty} e^{-\beta[(U/2)m(m-1)-\mu m]}$. The sums converge rapidly, reducing the finding of the phase boundary to the finding the solution of a nonlinear equation in one variable.

APPENDIX B: NONUNIVERSAL CONTRIBUTIONS

In order to see the collapse described in the main text, one needs to subtract off the nonuniversal contributions to the density (n_0) and compressibility (κ_0). One can readily calculate these nonuniversal contributions or, as described below, extract them from numerical or empirical measurements.

For example, consider the Bose-Hubbard model, where the nonuniversal contributions arise from the constant term $\mathcal{L}_0$ in Eq. (A1). This corresponds to the free-energy density of decoupled sites, implying that the nonuniversal contribution to any on-site observable is found by evaluating the observable at $t = 0$ and at the U, T, and μ of interest. One finds

$$n_0 = \frac{\sum_{n=0}^{\infty} n e^{-\beta\epsilon_n}}{\sum_{n=0}^{\infty} e^{-\beta\epsilon_n}}, \tag{B1}$$

with

$$\epsilon_n = \frac{U}{2}n(n-1) - \mu n. \tag{B2}$$

These sums converge quickly with n, and typically only a few terms are needed. In principle, one can also measure the function $n_0(T,\mu,U)$ by performing experiments at small t. In practice, there are a number of technical hurdles: equilibration is difficult in deep lattices [50], as is control and measurement of temperature [51], and for very deep lattices the Bose-Hubbard description breaks down [36,52–59].

As explained by Zhou and Ho [14], a more generic approach to accounting for the nonuniversal contributions is to expand about the quantum critical point. By construction, n_0 is an analytic function, $n_0(\mu,T) = \bar{n} + \mathcal{O}(\mu - \mu_c, T)$, where $\bar{n} = n(\mu_c,0)$ is a constant. Sufficiently close to the critical point, Eq. (3) simplifies to

$$T^{1-d/z}(\kappa - \bar{\kappa}) = \Upsilon\left(\frac{n-\bar{n}}{T^{d/z}}\right), \tag{B3}$$

and the only remnant of the nonuniversal functions n_0 and κ_0 are the constants $\bar{\kappa}$ and $\bar{n}$. In the examples in this paper, $\bar{\kappa} = 0$ and $\bar{n} = 0$ (vacuum to superfluid transition) or $\bar{n} = 1$ (n=1 Mott to superfluid transition). In circumstances where these constants are nontrivial, they may be extracted by fitting experimental or numerical data. Zhou and Ho give a discussion of carrying out this expansion to higher order.

Using Eq. (B3), we observe equally good collapse as we find from subtracting off the full n_0 in Eq. (B1). In addition to its simplicity, the expression in Eq. (B3) is completely in terms of simple constants and local observables. This can be contrasted with Eq. (B1), where one needs the central chemical potential in the trap. Additionally, Eq. (B3) is particularly powerful in that it applies even if one has only local equilibrium through the quantum critical regime [49].

APPENDIX C: CALCULATING DENSITY PROFILES OF ONE-DIMENSIONAL HARD-CORE BOSONS

For Fig. 2, we calculate our density profiles by mapping the one-dimensional, hard-core ($U \to \infty$), trapped lattice bosons described by the Hamiltonian

$$H = -t\sum_i \left[b_i^\dagger b_{i+1} + \text{H.c.} + \frac{U}{2}b_i^\dagger b_i^\dagger b_i b_i + (V_i - \mu)b_i^\dagger b_i\right], \tag{C1}$$

with harmonic trapping potential V_i, onto noninteracting fermions by the Jordan-Wigner transformation [60]:

$$f_i \equiv \left[\prod_{j<i}(1 - 2b_j^\dagger b_j)\right] b_i. \tag{C2}$$

Note that f_i and $f_i^\dagger$ satisfy the canonical anticommutation relation for fermions, $\{f_i, f_j^\dagger\} = \delta_{ij}$. This gives the noninteracting Fermi Hamiltonian:

$$H = \sum_i [-t(f_{i+1}^\dagger f_i + \text{H.c.}) + (V_i - \mu) f_i^\dagger f_i x]. \tag{C3}$$

We numerically find the single-particle eigenstates $\phi_i^{(\alpha)}$ with energy E_α. The bosonic density at site i is then equal to the fermionic density at site i by Eq. (C2), and thus

$$n_i = \sum_\alpha \frac{1}{e^{\beta E_\alpha} + 1}\left|\phi_i^{(\alpha)}\right|^2. \tag{C4}$$

APPENDIX D: UNIVERSALITY

As we have emphasized, our procedure allows the extraction of *universal* scaling curves from nonuniversal observables such as density profiles. Here, we make precise the meaning of this universality and offer a fairly detailed derivation of the scaling forms. This summarizes some of Fisher *et al.*'s [19] scaling arguments in the present notation (see also Sachdev's book [1]). First, we present the argument for a general observable. We additionally discuss the simplification that occurs when we specialize observables to the density and its derivatives, which take a simpler form due to the conservation of charge [40].

1. Scaling near a quantum critical point

First, we consider a general observable $\mathcal{O}(g_1, \ldots, g_n)$ that is a function of n coupling constants, chosen to vanish at the critical point. Using a coarse graining or renormalization group procedure, both $\mathcal{O}$ and the g_j's can be defined as functions of the scale ℓ.

Near the fixed point of a renormalization group flow, one generally has

$$g_j(\ell) = g_j \ell^{1/\nu_j} \tag{D1}$$

as $\ell \to \infty$. The exponents ν_j define scaling dimensions for the corresponding couplings g_j, and g_j is defined as $g_j \equiv g_j(\ell = 1)$.

Since the flow of coupling constants is defined to preserve the physics up to the scale,

$$\mathcal{O}[g_1(\ell), \ldots, g_n(\ell)] = \ell^{\alpha_\mathcal{O}} \mathcal{O}(g_1, \ldots, g_n), \tag{D2}$$

where $\alpha_\mathcal{O}$ is related to the scaling dimension of $\mathcal{O}$. We may solve Eq. (D2) for $\mathcal{O}(g_1, \ldots, g_n)$ and choose ℓ such that $\ell = (A/g_n)^{\nu_n}$ for some constant A, yielding

$$\mathcal{O}(g_1, \ldots, g_n) = A^{-\alpha_\mathcal{O}\nu_n} g_n^{\alpha_\mathcal{O}\nu_n} \mathcal{O}\left(\frac{g_1 A^{\nu_n/\nu_1}}{g_n^{\nu_n/\nu_1}}, \ldots, \frac{g_{n-1} A^{\nu_n/\nu_{n-1}}}{g_n^{\nu_n/\nu_{n-1}}}, A \right). \tag{D3}$$

Thus, we see that the dependence of $\mathcal{O}$ on all the coupling constants is captured, up to a nonuniversal scale in both $\mathcal{O}$ and its arguments (determined by A), by a universal function. This is frequently abbreviated

$$\mathcal{O}(g_1, \ldots, g_n) = g_n^{\alpha_\mathcal{O}\nu_n} \Psi_\mathcal{O}\left(\frac{g_1}{g_n^{\nu_n/\nu_1}}, \ldots, \frac{g_{n-1}}{g_n^{\nu_n/\nu_{n-1}}} \right),$$

with it implicitly understood that each argument and the overall factor has an associated nonuniversal scale. This is the sense in which our main text's equations should be understood as universal. We conventionally choose g_n to be the temperature T, obtaining

$$\mathcal{O}(g_1, \ldots, g_n) = A^{-\alpha_\mathcal{O}/z} T^{\alpha_\mathcal{O}/z} \mathcal{O}\left[\frac{g_1 A^{1/(z\nu_1)}}{T^{1/(z\nu_1)}}, \ldots, \frac{g_{n-1} A^{1/(z\nu_{n-1})}}{T^{1/(z\nu_{n-1})}}, A \right], \tag{D4}$$

since $T \propto \xi^{-z} \propto \ell^z$ by the definition of the dynamical critical exponent z.

2. Hyperscaling

The scaling dimension of $\mathcal{O}$ is related to the scaling dimension $\nu_\mathcal{O}$ of the conjugate coupling constant $g_\mathcal{O}$, where $\mathcal{O} = \partial\mathcal{F}/\partial g_\mathcal{O}$. Under a renormalization group transformation, the free energy scales as $\mathcal{F} \propto \ell^{d+z}$ for universality classes satisfying hyperscaling (as is generally the case for those relevant to quantum criticality). Thus, $\mathcal{O} \propto \ell^{d+z-1/\nu_\mathcal{O}}$, yielding $\alpha_\mathcal{O} = d + z - 1/\nu_\mathcal{O}$ and

$$\mathcal{O}(g_1, \ldots, g_n) = T^{1+d/z-1/(z\nu_\mathcal{O})} \mathcal{O}\left[\frac{g_1}{T^{1/(z\nu_1)}}, \ldots, \frac{g_{n-1}}{T^{1/(z\nu_{n-1})}} \right], \tag{D5}$$

where for notational clarity we have omitted the A's.

In the case of a conserved quantity, such as density, Sachdev [40] shows that one can relate $\nu_\mathcal{O}$ to z. Under an RG transformation, $n \propto \ell^d$, requiring $\alpha_n = d$. Thus $\nu_n = 1/z$ and

$$n_u = T^{d/z} \Psi_n\left[\frac{g_1}{T^{1/(z\nu_1)}}, \ldots, \frac{g_{n-1}}{T^{1/(z\nu_{n-1})}} \right]. \tag{D6}$$

Zhou and Ho'e expression [14] emerges directly from Eq. (D5) when μ is the only relevant coupling. As seen from Eq. (D6), their expression simplifies to $n_u = T^{d/z} \Psi_u(\frac{\mu-\mu_c}{T})$ regardless of the universality class of the phase transition.

APPENDIX E: QUANTUM MONTE CARLO PARAMETERS AND SIGNAL-TO-NOISE

We calculate the densities for the two-dimensional square lattice Bose-Hubbard model using worm algorithm quantum Monte Carlo algorithm [61] as implemented in the ALPS simulation package [31]. We performed a sufficient number of equilibration sweeps (10 000) and evaluation sweeps (30 000) to obtain accurate estimates of the density. Typical stochastic errors in the density were $\sim 0.1\%$, but these are amplified when we take derivatives to extract the compressibility. This stochastic error is comparable to imaging noise of radially averaged density profiles in real experiments [28] (1%). As seen in Fig. 3, our approach is robust against such noise. Even using the simplest finite difference approximations to derivatives—which greatly amplify noise—our technique provides accurate scaling curves up to noise levels of $\lesssim 1\%$. More sophisticated multipoint differentiation schemes are more robust to noise, and we expect these to be robust to noise of perhaps $\lesssim 5\%$. Even at the center of the cloud, some existing lattice experiments are already below this noise level and have demonstrated clean determination of both κ and n [28]. Furthermore, the noise level decreases with distance to the center due to trap averaging (although the chemical potential gradients eventually lead to breakdown of the Thomas-Fermi approximation, we find good agreement over a substantial portion of the cloud even, for example, for small of $N = 70$ 1D clouds). Systematic effects may be important as well, for example shot-to-shot total particle number fluctuations. These would have controlled, for example, by post-selection of particle number, and this will moderately increase running time for the experiments.

Over most of the parameter space simulated, we find that systematic errors from the finite equilibration time are significantly smaller than the stochastic errors. We explore possible systematic errors using two methods: (1) running with longer equilibration times and (2) a jackknife binning analysis. The simulations were carried out for a system size of 10×10 lattice sites. Our results were insensitive to the finite-size effects, except in the *classical* critical regime, mimicking the effects of a real trapping potential.

[1] S. Sachdev, *Quantum Phase Transitions* (Cambridge University Press, Cambridge, 2001).
[2] S. L. Sondhi, S. M. Girvin, J. P. Carini, and D. Shahar, Rev. Mod. Phys. **69**, 315 (1997).
[3] M. Vojta, Rep. Prog. Mod. Phys. **66**, 2069 (2003).
[4] S. Sachdev, in *Understanding Quantum Phase Transitions*, edited by Lincoln D. Carr (Taylor & Francis, Boca Raton, 2010).

[5] P. Coleman and A. J. Schofield, Nature (London) **433**, 226 (2005).
[6] I. Bloch, J. Dalibard, and W. Zwerger, Rev. Mod. Phys. **80**, 885 (2008).
[7] M. Imada, A. Fujimori and Y. Tokura, Rev. Mod. Phys. **70**, 1039 (1998).
[8] A. Georges, G. Kotliar, W. Krauth, and M. J. Rozenberg, Rev. Mod. Phys. **68**, 13 (1996).
[9] A. V. Chubukov, S. Sachdev, and J. Ye, Phys. Rev. B **49**, 11919 (1994).
[10] A. Sokol and D. Pines, Phys. Rev. Lett. **71**, 2813 (1993).
[11] S. Sachdev, Rev. Mod. Phys. **75**, 913 (2003).
[12] P. Gegenwart, Q. Si, and F. Steglich, Nat. Phys. **4**, 186 (2008).
[13] S. Sachdev and M. Müller, J. Phys. Condens. Matter **21**, 164216 (2009).
[14] Q. Zhou and T.-L. Ho, Phys. Rev. Lett. **105**, 245702 (2010).
[15] Shiang Fang, Chia-Ming Chung, Ping Nang Ma, Pochung Chen, and Daw-Wei Wang, Phys. Rev. A **83**, 031605(R) (2011).
[16] Xiwen Guan and Tin-Lun Ho, e-print arXiv:1010.1301.
[17] Xiangguo Yin, Xi-Wen Guan, Shu Chen, and Murray T. Batchelor, e-print arXiv:1101.2494; Murray T. Batchelor, Angela Foerster, Xiwen Guan, and Carlos C. N. Kuhn, J. Stat. Mech. (2010) P12014.
[18] Xibo Zhang, Chen-Lung Hung, Shih-Kuang Tung, Nathan Gemelke, and Cheng Chin, New J. Phys. **13**, 045011 (2011).
[19] M. P. A. Fisher, P. B. Weichman, G. Grinstein and D. S. Fisher, Phys. Rev. B **40**, 546 (1989).
[20] D. Jaksch, C. Bruder, J. I. Cirac, C. W. Gardiner, and P. Zoller, Phys. Rev. Lett. **81**, 3108 (1998).
[21] Stefan Wessel, Fabien Alet, Matthias Troyer, and G. G. Batrouni, Phys. Rev. A **70**, 053615 (2004).
[22] Q. Zhou, Y. Kato, N. Kawashima, and N. Trivedi, Phys. Rev. Lett. **103**, 085701 (2009).
[23] M. Köhl, T. Donner, S. Ritter, T. Bourdel, A. Ottl, F. Brennecke, and T. Esslinger, in *Advances in Solid State Physics*, 79 (2008).
[24] S. Trotzky, L. Pollet, F. Gerbier, U. Schnorrberger, I. Bloch, N. V. Prokofev, B. Svistunov, and M. Troyer, Nature Physics **6**, 998 (2010).
[25] L. Pollet, N. V. Prokof'ev, and B. V. Svistunov, Phys. Rev. Lett. **104**, 245705 (2010).
[26] Sylvain Nascimbène, Nir Navon, Frédéric Chevy, and Christophe Salomon, New J. Phys. **12**, 103026 (2010); Nir Navon, Sylvain Nascimbène, Frédéric Chevy, and Christophe Salomon, Science **328**, 729 (2010).
[27] T. Ho and Q. Zhou, Nat. Phys. **6**, 131 (2010).
[28] N. Gemelke, X. Zhang, C. Hung, and C. Chin, Nature (London) **460**, 995 (2009).
[29] Thibaut Jacqmin, Julien Armijo, Tarik Berrada, Karen Kheruntsyan, and Isabelle Bouchoule, e-print arXiv:1103.3028; J. Armijo, T. Jacqmin, K. V. Kheruntsyan, and I. Bouchoule, Phys. Rev. Lett. **105**, 230402 (2010); Phys. Rev. A **83**, 021605(R) (2011).
[30] S. Sachdev and E. R. Dunkel, Phys. Rev. B **73**, 085116 (2006).
[31] A. Albuquerque *et al.*, J. Magn. Magn. Mater. **310**, 1187 (2007).
[32] R. Joerdens, N. Strohmaier, K. Günter, H. Moritz, and T. Esslinger, Nature (London) **455**, 204 (2008).
[33] U. Schneider, L. Hackermüller, S. Will, Th. Best, I. Bloch, T. A. Costi, R. W. Helmes, D. Rasch, and A. Rosch, Science **322**, 1520 (2008).
[34] C. Schori, T. Stöferle, H. Moritz, M. Köhl, and T. Esslinger, Phys. Rev. Lett. **93**, 240402 (2004).
[35] D. Clément, N. Fabbri, L. Fallani, C. Fort, and M. Inguscio, Phys. Rev. Lett. **102**, 155301 (2009).
[36] Gretchen K. Campbell, Jongchul Mun, Micah Boyd, Patrick Medley, Aaron E. Leanhardt, Luis G. Marcassa, David E. Pritchard, and Wolfgang Ketterle, Science **313**, 649 (2006).
[37] A. Abanov and A. V. Chubukov, Phys. Rev. Lett. **84**, 5608 (2000).
[38] M. A. Metlitski and S. Sachdev, Phys. Rev. B **82**, 075128 (2010).
[39] A. J. Schofield, Phys. Status Solidi B **247**, 563 (2010).
[40] S. Sachdev, Z. Phys. B **94**, 469 (1994).
[41] S. A. Hartnoll, P. K. Kovtun, M. Muller and S. Sachdev, Phys. Rev. B **76**, 144502 (2007).
[42] Y. Kato, Q. Zhou, N. Kawashima, and N. Trivedi, Nat. Phys. **4**, 617 (2008).
[43] M. Ueda and Y. Kawaguchi, e-print arXiv:1001.2072 (2010).
[44] T. Lahaye, C. Menotti, L. Santos, M. Lewenstein, and T. Pfau, Rep. Prog. Phys. **72**, 126401 (2009).
[45] W. Ketterle and M. W Zwierlein, in *Ultracold Fermi Gases, Proceedings of the International School of Physics "Enrico Fermi," Course CLXIV, Varenna, 20–30 June,* 2006, edited by M. Inguscio, W. Ketterle, and C. Salomon (IOS Press, Amsterdam, 2008).
[46] Yean-an Liao, Ann Sophie C. Rittner, Tobias Paprotta, Wenhui Li, Guthrie B. Partridge, Randall G. Hulet, Stefan K. Baur, and Erich J. Mueller, Nature (London) **467**, 567 (2010).
[47] Steffen P. Rath, Tarik Yefsah, Kenneth J. Günter, Marc Cheneau, Rémi Desbuquois, Markus Holzmann, Werner Krauth, and Jean Dalibard, Phys. Rev. A **82**, 013609 (2010).
[48] M. Campostrini and E. Vicari, Phys. Rev. Lett. **102**, 240601 (2009); Phys. Rev. A **81**, 063614 (2010); **81**, 023606 (2010).
[49] Stefan S. Natu, Kaden R. A. Hazzard, Erich J. Mueller, Phys. Rev. Lett. **106**, 125301 (2011).
[50] C. L. Hung, X. Zhang, N. Gemelke, and C. Chin, Phys. Rev. Lett. **104**, 160403 (2010).
[51] David M. Weld, Patrick Medley, Hirokazu Miyake, David Hucul, David E. Pritchard, and Wolfgang Ketterle, Phys. Rev. Lett. **103**, 245301 (2009); Stefan S. Natu and Erich J. Mueller, Phys. Rev. A **82**, 013612 (2010).
[52] O. E. Alon, A. I. Streltsov, and L. S. Cederbaum, Phys. Rev. Lett. **95**, 030405 (2005).
[53] J. Li, Y. Yu, A. M. Dudarev, and Q. Niu, New J. Phys. **8**, 154 (2006).
[54] G. Mazzarella, S. M. Giampaolo, and F. Illuminati, Phys. Rev. A **73**, 013625 (2006).
[55] A. Smerzi and A. Trombettoni, Phys. Rev. A **68**, 023613 (2003).
[56] P. R. Johnson, E. Tiesinga, J. V. Porto, and C. J. Williams, New J. Phys. **11**, 093022 (2009).
[57] J. Larson, A. Collin, and J. P. Martikainen, Phys. Rev. A **79**, 033603 (2009).
[58] K. R. A. Hazzard and E. J. Mueller, Phys. Rev. A **81**, 031602 (2010).
[59] Sebastian Will, Thorsten Best, Ulrich Schneider, Lucia Hackermüller, Dirk-Sören Lühmann, and Immanuel Bloch, Nature (London) **465**, 197 (2010).
[60] P. Jordan and E. Wigner, Z. Phys. **47**, 631 (1928).
[61] N. V. Prokof'ev, B. V. Svistunov, and I. S. Tupitsyn, Phys. Lett. A **238**, 253 (1998).